(Received 21 March 2026, Accepted 20 April 2026, Scheduled 25 June 2026)

Design and Experimental Validation of an Ultra-Thin Compact 2.4 GHz Microstrip Antenna for ZigBee-Based IoT Network

Kumar V. Srivastava*, Rajan Mishra, Rajeev K. Chauhan, and Praveen K. Rao

Department of Electronics and Communication Engineering
Madan Mohan Malaviya University of Technology, Gorakhpur 273010, U.P., India

ABSTRACT: The rapid advancement of wireless communication technologies and the Internet of Things (IoT) has led to a substantial demand for energy-efficient and miniature antennas for short-range wireless data communication. This paper presents the design, fabrication, and experimental authentication of a small, ultra-thin, microstrip patch antenna operating at 2.4 GHz for ZigBee-based IoT applications. The antenna was designed on a cost-effective FR4 epoxy substrate with dimensions of $20 \times 40 \times 0.8\,\text{mm}^3$, facilitating easy integration into compact sensors and embedded devices. A step-by-step parametric optimization methodology was employed to analyze the impact of various evolution phases, ground plane length, and slot width of the proposed antenna on S_{11}, peak gain, and radiation efficiency. These parameters were evaluated via simulation and authenticated by laboratory measurements. The results exhibit good impedance matching with a measured S_{11} of -41 dB and a bandwidth of 150 MHz for the ZigBee network. The antenna achieves a measured peak gain of 2.46 dBi, as well as 79% of radiation efficiency. To substantiate practical implementation, the antenna was integrated with a ZigBee-enabled network, and over-the-air (OTA) experiments are demonstrated using Received Signal Strength Index (RSSI) measurements. The results verify the short-range communication suitable for IoT-based network systems. The proposed design offers a miniature, low-profile, and cost-effective antenna solution for modern ZigBee-enabled IoT architectures.

1. INTRODUCTION

In recent years, the rapidly growing Internet of Things (IoT) has drastically increased the demand for a reliable wireless communication technology that consumes low energy, is easily integrated into miniature IoT devices, and smoothly transmits data. IoT-enabled devices are extensively deployed in applications such as smart homes, smart cities, industrial automation, and environmental monitoring. Among the numerous wireless technologies available, like ZigBee, Long Range (LoRa), Wi-Fi, Bluetooth, Radio Frequency Identification (RFID), Near Field Communication (NFC), and drone systems, ZigBee has emerged as a premier standard. Among the numerous wireless technologies available, such as ZigBee, Long Range (LoRa), Wi-Fi, Bluetooth, Radio Frequency Identification (RFID), Near Field Communication (NFC), and drone systems, ZigBee has emerged as a premier standard, based on the IEEE 802.15.4 standard, and is broadly adopted because of its minimal power utilization, capability of making mesh networks, and suitability for short-range wireless sensor networks.

ZigBee technology has been developed to establish low-power personal area networks (PANs), extensively used for short-range communications in applications such as smart cities, smart offices, smart buildings, real-time monitoring systems, and industrial automation [1].

Designing methodology of antenna is a vital component in these wireless communication networks, as it directly enhances performance, reliability, efficiency, and scalability. Miniaturization and adequate bandwidth are key constraints to uphold fast, real-time communication in IoT devices. Microstrip antennas are particularly suitable because of their compact geometry, planar profile, and ease of integration with IoT hardware [2].

For IoT-enabled devices, a variety of antennas have been designed to achieve a gain of 1.72 dBi and a radiation efficiency of 96% with -18 dB return loss [3]. Likewise, Ultra High Frequency (UHF) microstrip antennas are extensively utilized in IoT connectivity using Radio Frequency Identification (RFID) applications due to their low profile and easy fabrication on a standard FR4 substrate [4]. Targeting IoT applications, a 2.4 GHz, automatic radiation pattern reconfigurable 3D antenna has been developed using a PIN diode [5]. For the fifth generation communication technology with near-body applications, a Multiple-Input Multiple-Output (MIMO) antenna has been designed at 2.4 GHz to achieve a low Specific Absorption Rate (SAR) of 0.58 W/kg [6].

In recent literature, an energy-harvested Vivaldi endfire antenna array embedded with nona-band rectifiers for boosting the power of the antenna makes it highly efficient around 74% [7]. For a healthcare monitoring system, an antenna designed at 2.4 GHz and 5.8 GHz uses Rogers Duroid RO3003 as a substrate material to support multiple integrated sensors [8].

Some other antennas designed for Wi-Fi and WiMAX applications use Left Temple Antenna (LTA) and for Bluetooth application use Right Temple Antenna (RTA), also fabricated on FR4 substrate [9]. In recent techniques for bandwidth enhance-

* Corresponding author: Kumar Vaibhav Srivastava (kumarvaibhav19@gmail.com).

ment and size reduction, a frequency-reconfigurable multiband antenna incorporates a 4×4 Artificial Magnetic Conductor (AMC) surface combined with a Defected Ground Structure (DGS) supporting surface wave suppression [10]. To overcome the Industrial, Scientific, and Medical (ISM) band shortcomings of low gain and narrow bandwidth, designs utilizing foam substrate [11] or mirror-image radiator arrangements yielding high gain [12] have been proposed. Other specialized designs include wearable off-body antennas exhibiting high impedance matching [13] and energy-harvesting Vivaldi antennas integrated with layered rectifiers to power ZigBee modules over considerable distances [7, 14]. To support diverse IoT ecosystems, recent literature has explored multistranded planar architectures, such as the octahedron-shaped antenna [15] designed to consolidate UHF, microwave, and sub-6 GHz bands into a single device. Some other novel approaches to permeating IoT space constraints encompass integrating radiating elements directly into IoT-enabled devices. For example, an optically invisible antenna embedded within an Organic Light-Emitting Diode (OLED) touch display panel has been designed for IoT applications [16]. However, these transparent and display-integrated designs often demand specialized materials and complex fabrication procedures. Additionally, the expansion of body-centric IoT networks tends to be highly customized, conformal designs, such as an antenna easily integrated into a handbag zipper [17]. Other major miniaturization tactics for the 2.4 GHz ISM band involve modifying the fundamental shape of the radiating element to enhance impedance bandwidth for small-size IoT devices [18]. In the pursuit of viable IoT deployments, current efforts have also shown eco-friendly substrates, such as an ultra-thin compact monopole designed on Tencel textile specifically for ZigBee-enabled systems [19]. Likewise, folded strip and slot structures have been developed to expand the bandwidth for WLAN applications [21]. A standard graphical representation of a ZigBee sensor network, exhibiting the data communication path from the sensor node to the end user, is illustrated in Fig. 1.

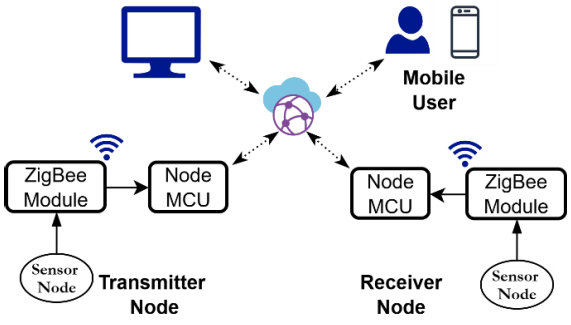

FIGURE 1. Data flow diagram of ZigBee network.

In spite of these advancements, many existing 2.4 GHz antennas have relatively thick substrates (1.6 mm) or larger patches, which inhibit their integration into the latest, ultra-slim IoT sensor networks. So, the novelty of this work lies in the design, implementation, and practical validation of an ultra-slim (0.8 mm) miniature antenna customized for a ZigBee network. By systematically transforming the radiating patch and partial ground plane, the major contributions are as follows:

- The design of an ultra-thin microstrip antenna resonating at 2.4 GHz with miniature dimensions of $20 \times 40 \times 0.8\,\text{mm}^3$ is appropriate for low-profile IoT applications.
- A comprehensive parametric analysis was performed to investigate the effects of ground plane length and slot width on antenna parameters like S_{11}, peak gain, and radiation efficiency.
- The fabrication and experimental ratification of the proposed antenna in an anechoic chamber measurement setup authenticate the simulated parameters and surface current distribution.
- The practical setup of the proposed antenna with a ZigBee module and authentication of real-world communication performance uses Received Signal Strength Indicator (RSSI) measurements.

Although several antennas have been reported for ZigBee applications, many of them rely on thick substrates or complex geometries, which increase fabrication complexity and limit their deployment in compact IoT devices.

2. ANTENNA GEOMETRY AND DESIGN METHODOLOGY

2.1. Antenna Geometry

The suggested ultra-slim, microstrip antenna is designed to operate in the 2.4 GHz for ZigBee-enabled IoT applications. The dimensions of the antenna are highly compact, engaging a volume of $20 \times 40 \times 0.8\,\text{mm}^3$. It is fabricated on an affordable substrate FR4 with a dielectric constant (ε_r) of 4.4, a loss tangent ($\tan\delta$) of 0.02, and an ultra-thin thickness of 0.8 mm.

The patch is located on the upper layer, while an amended partial ground plane is etched on the bottom layer of the antenna substrate. A 50 Ω coaxial probe feed is used to excite the antenna, with the feeding point positioned to accomplish optimal impedance matching. The schematic of the working antenna, including the top patch and bottom ground plane, is shown in Fig. 2, specifying the key parametric variables (L_1 to L_5). The complete substrate footprint ($L_S \times W_S$) and the ground plane attribute ($L_G \times W_G$) are detailed in Table 1.

2.2. Design Evolution and Methodology

To achieve an operating frequency at 2.4 GHz under such a physical structure barrier and ultra-thin profile, the antenna goes through a methodical evolution process. The fundamental challenge of employing a 0.8 mm substrate is the heightened capacitive coupling between the upper radiating patch and the bottom ground plane, which restricts the bandwidth and improves the resonant frequency. To offset this, physical adaptations were implemented across four distinct phases (Phase I to Phase IV), as shown in Fig. 3.

- **Phase I (Conventional Patch):** In the initial phase, a rectangular patch with full ground was considered. Because

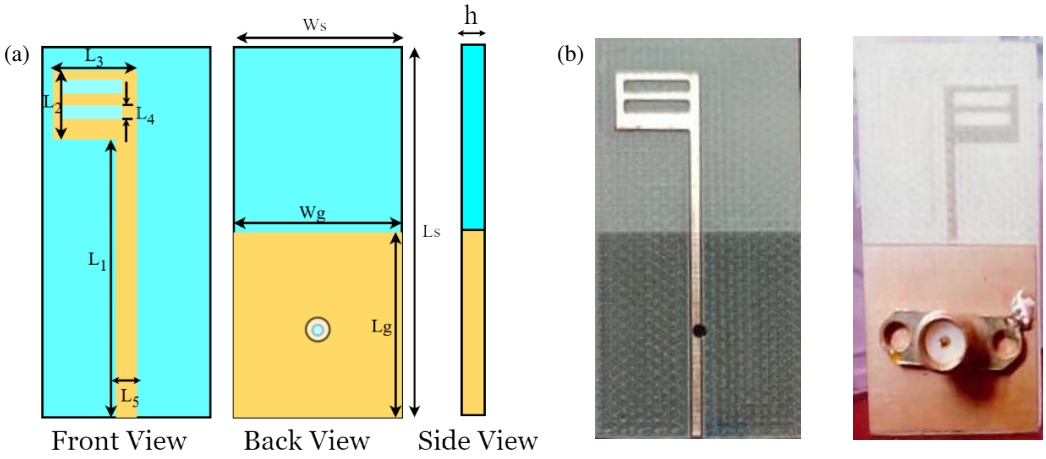

FIGURE 2. Schematic diagram of the proposed antenna.

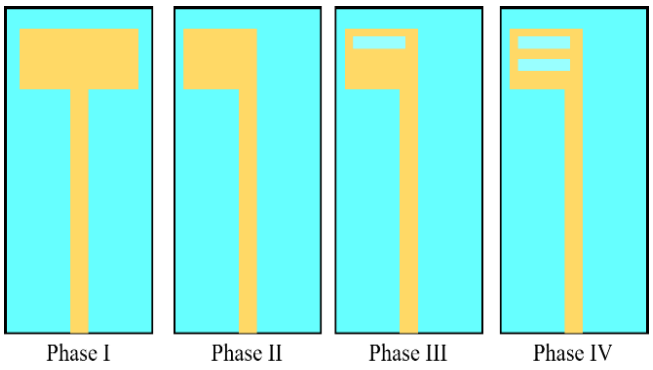

FIGURE 3. Phase-wise evolution of the proposed antenna.

of the limited dimension of $20 \times 40\,\text{mm}^2$, the resonant frequency was much higher than the targeted 2.4 GHz band, and the impedance matching was not so good.

- **Phase II (Half Rectangular Shape):** The second phase intended to enhance the impedance matching and lower the Q-factor innate to the 0.8 mm FR4 substrate, and the ground plane was curtailed into a partial ground plane. This reformation altered the fringing fields and improved the bandwidth.
- **Phase III (Introduction of Slots):** To adjust the resonant frequency without any increase in the overall dimension, rectangular slots were cut into the upper patch. These slots force the surface currents to follow a meandering path, thereby increasing the electrical length of the antenna, thus, a significant shift in the resonant frequency toward the 2.4 GHz band.
- **Phase IV (Ground Modification and Final Design):** In this phase, the slot structures and the length of the ground plane were optimized parametrically to their targeted values. This particular setting balanced the capacitive and inductive reactance, getting a better return loss at resonance at 2.4 GHz and a strong radiation profile adaptable for ZigBee networks.

TABLE 1. Parametric details of the working antenna.

Parameters of Proposed Antenna			
Measurement of Patch (Front View)		Measurement of Ground Plane and Substrate (Back View & Side View)	
L_1	28 mm	L_S	40 mm
L_2	8 mm	W_S	20 mm
L_3	6 mm	L_G	20 mm
L_4	2 mm	W_G	20 mm
L_5	2 mm	h	0.8 mm

3. PARAMETRIC OPTIMIZATION

To achieve the aimed operating frequency, 2.4 GHz, the suggested antenna was designed through a step-by-step, phase-wise evolution process. As illustrated in Fig. 3, the design evolved from a basic rectangular patch to the final slotted structure. In this evolution procedure, antenna performance, including return loss, peak gain, and radiation efficiency, was examined to analyze the impact of each structural alteration. Table 2 summarizes the phase-wise progression of important performance metrics, including operating frequency, return loss (S_{11}), peak gain, and radiation efficiency. This iterative structure evolution permitted the accurate tuning of the physical parameters, finally achieving optimal performance of the designed antenna.

Figure 4 shows the return-loss (S_{11}) behaviors across Phases I to IV. Due to the strict overlap in the simulated results, different line thicknesses and colors are utilized for clarity (Phase II: thick red line; Phase III: medium green line; Phase IV: thin blue line). At the aimed operating frequency of 2.4 GHz, Phase IV exhibits an optimized return loss, showing optimal impedance matching and minimal signal reflection compared with the preceding iterations. As illustrated in Fig. 5, the peak gain is increasingly developed from Phase I to Phase IV. By attaining its optimal peak gain at exactly 2.4 GHz, Phase IV ensures strong link stability and improved signal transmission for IoT appli-

TABLE 2. Phase-wise parametric analysis of the proposed antenna.

Evolution Phase of Antenna	Operating Frequency (GHz)	S_{11} (dB)	Radiation Efficiency %	Peak Gain (dBi)
Phase I	2.2	−22	76	2.40
Phase II	2.4	−39	78	2.32
Phase III	3.1	−40	77	2.29
Phase IV	2.4	−52	79	2.47

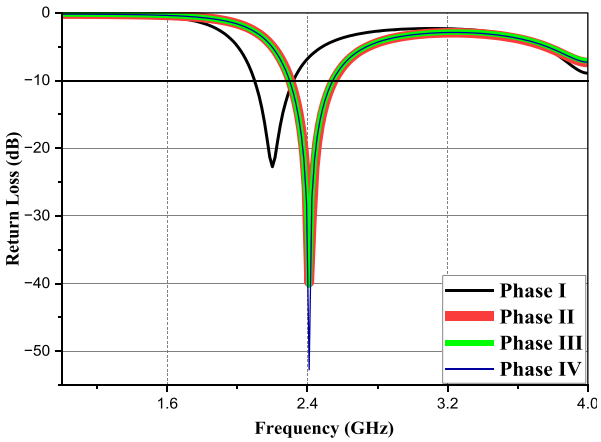

FIGURE 4. Return loss measured for all phases of the antenna.

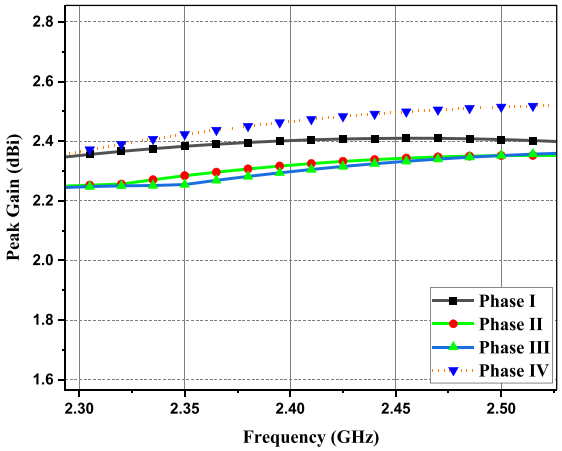

FIGURE 5. Peak gain measurement of each phase.

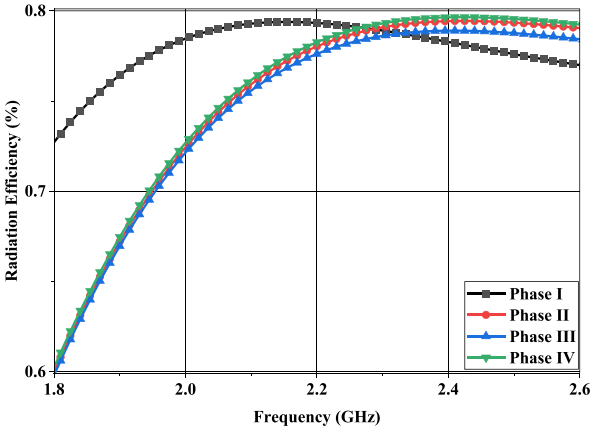

FIGURE 6. Radiation efficiency for all phases of the antenna.

cations. Similarly, the radiation efficiency, plotted in Fig. 6, illustrated a notable enhancement during the final optimization phase, authenticating the effectiveness of the structural modifications.

The next important parameter for the attention is the modification of the length of the ground plane, as demonstrated in Fig. 7, which is a vital aspect of antenna design owing to its impact on the input impedance. This parameter affects the performance extensively by affecting how well the antenna can be matched to its transmission-line impedance.

The length of the ground plane (L_G) plays a vital role in dictating the resonant nature and impedance bandwidth of the proposed antenna. To tune the required operating frequency, L_G was parametrically swept from 5 mm to 25 mm in increments of 5 mm. The following return loss (S_{11}) parameters for each variation are plotted in Fig. 8, exhibiting the antenna's impedance matching performance across the 1 to 4 GHz band.

The alteration in the antenna parameters, such as return loss, peak gain, and radiation efficiency, by varying the length of the ground plane is shown in Figs. 8 and 9, respectively. As L_G is changed from 5 mm to 25 mm, the resonant frequency shifts to higher values. Optimal impedance matching is reached at $L_G = 20$ mm, which shows a return loss of approximately −51 dB. On the other hand, the analysis of the peak gain in 2.25 GHz to 2.55 GHz band (Fig. 9) discloses an upward trend with increasing frequency and ground plane length. The optimum peak gain of nearly 2.7 dBi is seen at $L_G = 25$ mm, showing a good design trade-off between maximum peak gain and optimal impedance matching.

Fig. 10 illustrates the impact of the ground plane length (L_G) on the radiation efficiency of the antenna across the 2.0 GHz to 2.5 GHz spectrum. The simulated results present very efficient radiation characteristics, approximately between 78% and 79% for the targeted Zigbee band. Table 3 presents antenna operating parameters, including the return loss (S_{11}), radiation efficiency, and peak gain, for various lengths of the ground plane. This verifies that the structural alterations on the ground plane do not introduce excessive conduction or dielectric losses, ensuring maximum power radiation.

Also, the rectangular slot width (L_5) serves as a major setting parameter for the impedance bandwidth of the antenna. To know its impact, L_5 was parametrically changed from 1.0 mm

TABLE 3. Parametric analysis of the proposed antenna for various ground planes.

Length of Ground Plane L_G (mm)	Operating Frequency (GHz)	S_{11} Parameter (dB)	Radiation Efficiency %	Peak Gain (dBi)
5	2.27	−6	76	2.19
10	2.23	−15	77	2.01
15	2.30	−16	78	2.26
20	2.41	−52	79	2.46
25	2.49	−8	73	2.16

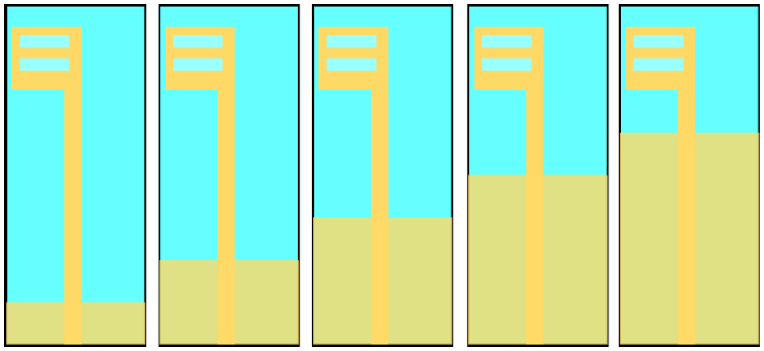

FIGURE 7. Length of ground plane variation.

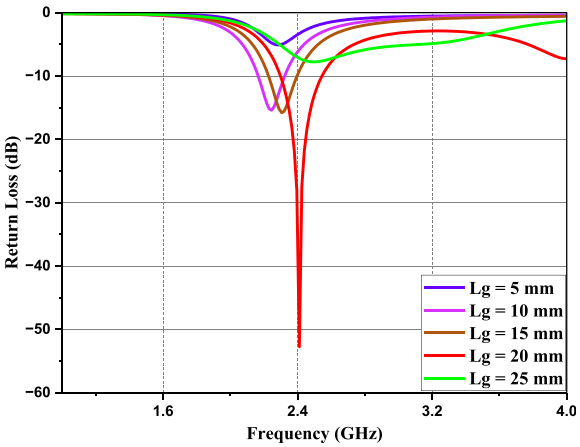

FIGURE 8. Return loss measured for multiple ground-plane lengths.

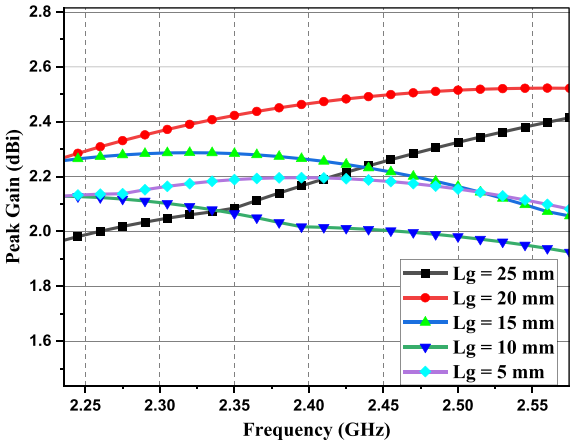

FIGURE 9. Peak gain for various ground-plane lengths.

to 2.5 mm. Because amending the slot width directly alters the surface current direction, step-by-step settlements to L_5 provide more control over the return loss, peak gain, and radiation efficiency, making it important for satisfying the rigid performance requirements of the ZigBee band.

Figures 11, 12, and 13 present the parametric analysis of the slot width (L_5) on S_{11}, peak gain, and radiation efficiency, respectively, of the antenna. As L_5 is decreased from 2.5 mm to 1.0 mm, the peak gain demonstrates a steady increase, reaching its maximum value at $L_5 = 1.3$ mm. Similarly, the radiation efficiency achieves its optimal performance exactly at the target 2.4 GHz frequency for the same dimension. Consequently, $L_5 = 1.3$ mm was selected as the optimal slot width, as it simultaneously maximizes both gain and efficiency while maintaining deep impedance matching. Table 4 outlines the key characteristics of the antenna, including the return loss (S_{11}), radiation efficiency, and peak gain, for various slot widths.

4. RESULTS AND DISCUSSION

Parametric analysis of the suggested antenna has been conducted to determine the optimum design parameters that achieve the desired performance. The antenna was fabricated and measured in an anechoic chamber shown in Fig. 14, demonstrating strong impedance matching with a return loss of −41 dB.

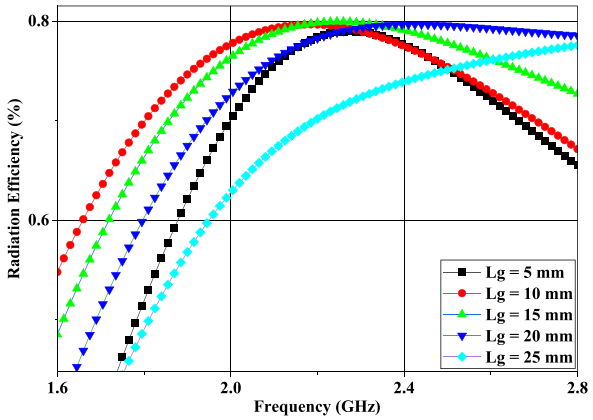

FIGURE 10. Radiation efficiency for different ground-plane lengths.

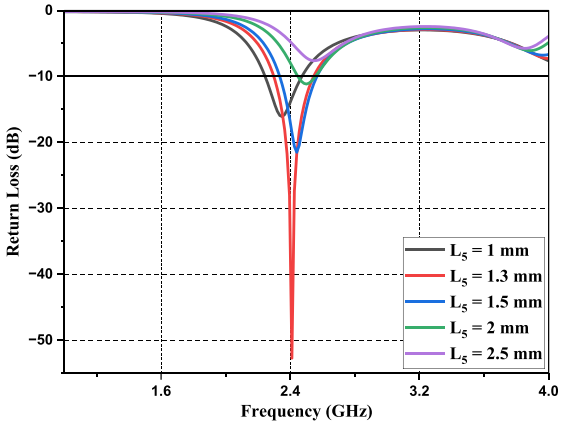

FIGURE 11. Return loss variation for slot width L_5.

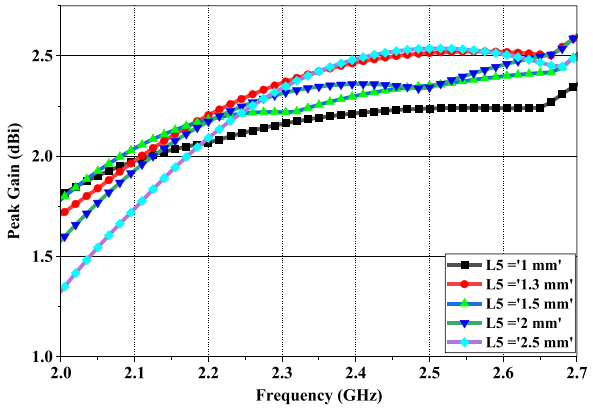

FIGURE 12. Peak gain variation for slot width L_5.

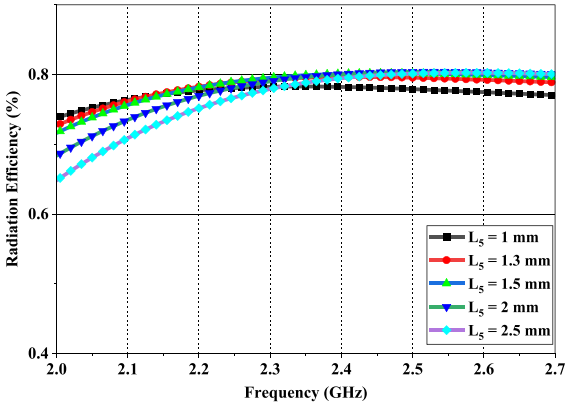

FIGURE 13. Radiation efficiency variation for slot width L_5.

FIGURE 14. Measurement of antenna in an anechoic chamber.

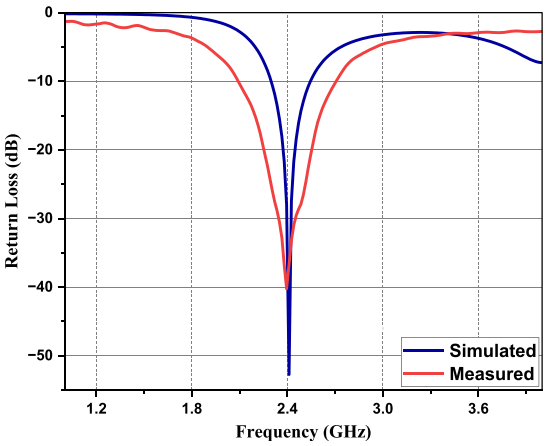

FIGURE 15. Simulated and measured return losses.

The simulated and measured S_{11} characteristics of the suggested antenna are exhibited in Fig. 15. Both results indicate resonance near 2.4 GHz, with simulated S_{11} of -52 dB and measured S_{11} of -41 dB. The minor deviation between simulated and measured responses is attributed to fabrication tolerances, connector losses, and dielectric variation in the FR-4 substrate. After lab measurement, simulated and measured results are compared in Table 5, which indicates that the proposed antenna has high efficiency with strong bandwidth performance.

The suggested ZigBee antenna's parameters are depicted in Fig. 16, with particular attention paid to radiation efficiency and peak gain over the frequency range of 2.0 GHz to 2.5 GHz.

Simulated results indicate that both peak gain and radiation efficiency are optimized perfectly at the 2.4 GHz target frequency, achieving 1.90 dBi and 79%, respectively. The effective efficiency is unchanged throughout the studying range of frequency from 2.0 GHz to 2.8 GHz. This simultaneous optimization of peak gain and radiation efficiency demonstrates that the ultra-thin FR4 design has minimal power loss, with its high viability and strong link stability for the network deployed using a ZigBee module.

TABLE 4. Parametric analysis of the proposed antenna for different slot widths L_5.

Width of the Slot L_5 (mm)	Operating Frequency (GHz)	S_{11} Parameter (dB)	Radiation Efficiency %	Peak Gain (dBi)
1.0	2.34	−16	78	2.22
1.3	2.40	−52	79	2.46
1.5	2.43	−21	79	2.30
2.0	2.50	−11	79	2.35
2.5	2.55	−8	78	2.48

TABLE 5. Performance of the proposed antenna on simulated and measured standards.

Proposed Antenna	Operating Frequency (GHz)	S_{11} (dB)	Radiation Efficiency %	Peak Gain (dBi)
Simulated	2.4	−51	79	1.90
Measured	2.4	−41	78	2.46

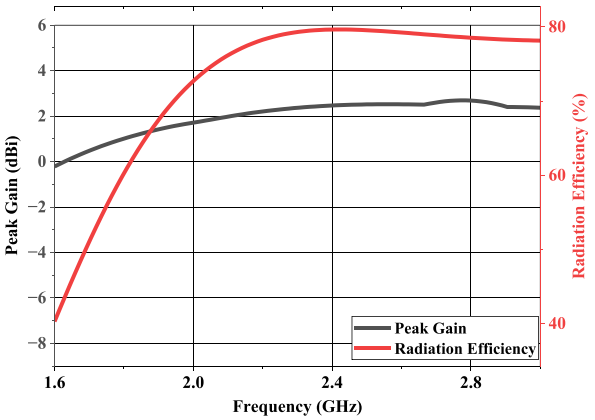

FIGURE 16. Peak gain and radiation efficiency of the proposed antenna.

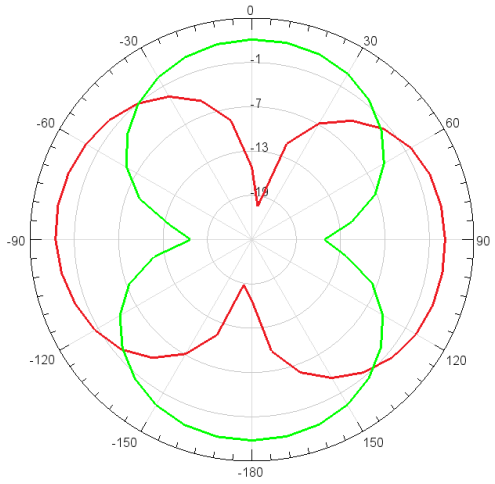

FIGURE 17. E-plane and H-plane far-field patterns.

Figure 17 exhibits the simulated 2D polar radiation patterns of the proposed antenna at resonant frequency 2.4 GHz. The H-plane shows a strong, quasi-omnidirectional structure, validating uniform azimuthal signal coverage, whereas the E-plane illustrates a regular dumbbell shape, with maximum broadside gain attaining maximum gain at approximately 2.46 dBi along 0° and 180°, with evident structural nulls at ±90°. This symmetric and rigidly aligned radiation pattern authenticates competent spatial energy distribution, making the design suitable for a stable ZigBee network.

Figure 18(a) exhibits the simulated electric field (E-field) distribution of the suggested antenna at 2.4 GHz. Because the working antenna utilizes an ultra-thin 0.8 mm FR4 substrate, the capacitive coupling between the patch and the ground plane is mainly heightened compared to regular 1.6 mm height. Hence, the surface currents are limited, with the maximum current density concentrated mainly along the edges of the patch and internal slots. This strong edge restraint limits the natural fringing fields, which lowers the impedance matching. On the other hand, by optimizing the slot widths and ground plane length, the resonant current path is improved. This strategic current meandering compensates for the high Q-factor inherent to ultra-thin substrates, permitting the antenna to maintain good impedance matching and radiation efficiency at the targeted 2.4 GHz ZigBee spectrum.

The simulated magnetic field (H-field) distribution at the aimed 2.4 GHz resonant frequency is illustrated in Fig. 18(b). Intense magnetic-field concentrations are confined at the feed junction and the inner edges of the patch, signifying effective power coupling into the radiating structure. Additionally, the lower-intensity regions detected on the ground plane validate its minimal, non-disruptive contribution to the overall near-field interactions. This effective, balanced current distribution is directly joined with the antenna's optimized peak gain of 2.46 dBi, verifying stable and strong power transfer for ZigBee-based systems.

The 3D radiation pattern illustrated in Fig. 19 for the suggested antenna at resonant frequency 2.4 GHz is plotted in a spherical coordinate system, where the radial distance from the origin directly corresponds to the absolute total gain measured in dBi. The antenna demonstrates a characteristic toroidal ra-

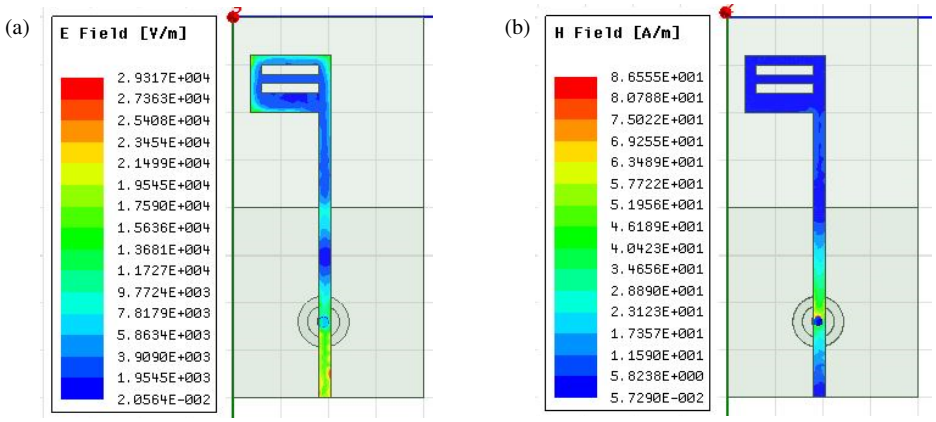

FIGURE 18. Current distribution for (a) E-field and (b) H-field of the proposed antenna.

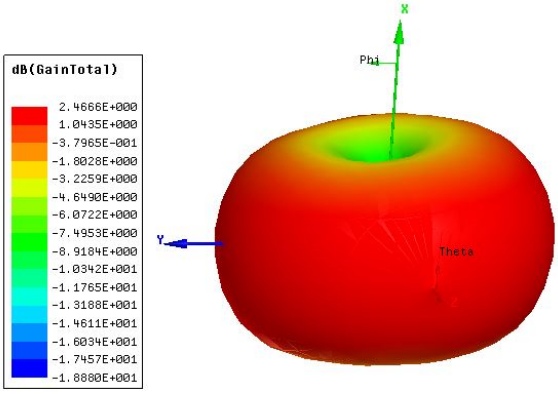

FIGURE 19. Three-dimensional radiation pattern of the working antenna.

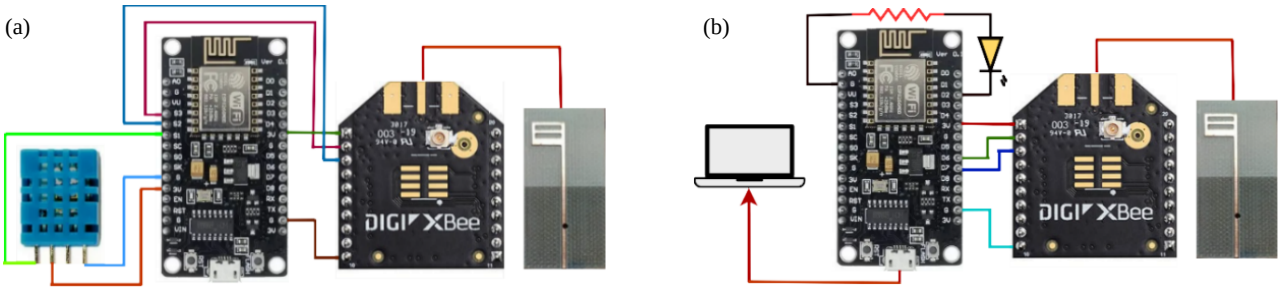

FIGURE 20. Circuit diagram of (a) transmitter and (b) receiver node of the ZigBee network.

diation pattern. Maximum radiation is concentrated along the primary radiating planes, attaining a peak simulated gain of 2.46 dBi. This quasi-omnidirectional profile confirms the antenna's structural efficiency and its suitability for establishing reliable ZigBee-based IoT networks.

To validate practical data transmission, temperature and humidity data obtained from a Digital Humidity and Temperature (DHT) sensor were transmitted using the proposed antenna integrated into the transmitter node of a ZigBee network (Fig. 20(a)). This signal was successfully captured by the receiver node (Fig. 20(b)), which was identically equipped with the proposed antenna. To ensure user accessibility, the received data was subsequently routed through cloud services directly to a mobile Blynk application.

Received Signal Strength Indicator (RSSI) is one of the key parameters for evaluating and validating the real-world performance of the proposed antenna. Furthermore, the Received Signal Strength Indicator (RSSI) was evaluated to validate the

TABLE 6. Measurement of RSSI at different locations.

Distance (meter)	RSSI (dBm)	Packet Success %	Communication Status
01	−65	99	Excellent
05	−71	95	Very Stable
10	−78	89	Stable
15	−87	82	Moderate
20	−92	72	Acceptable

TABLE 7. Comparison of various antennas designed for IoT applications.

Reference	Dimension (mm^2)	Operating Frequency (GHz)	Substrate	S_{11} (dB)	Gain (dBi)	Network Validation
[3]	20×45	2.34	FR4	-18	1.72	YES
[7]	41×44	2.4	Rogers Duroid RO3003	-21	4.82	YES
[16]	130×90	2.42	Polyguide	-18	3.29	NO
[17]	44.1×32.42	2.4	Polyethylene Terephthalate	-21	-1.36	NO
[18]	20×20	2.44	Textile Material	-21	5.00	NO
[19]	40×10	2.4	FR4	-19.11	1.34	NO
[20]	28.3×34.5	2.45	RO 3003	-20	2.1	YES
[21]	9.2×6.5	2.39	FR4	-13	NA	NO
Proposed antenna	20×40	2.4	FR4	-41	2.46	YES

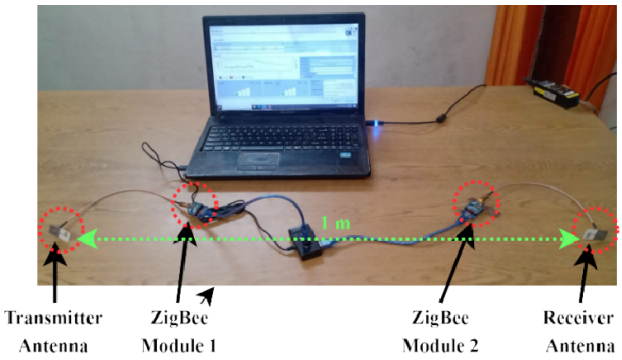

FIGURE 21. Range test setup of the proposed ZigBee antenna.

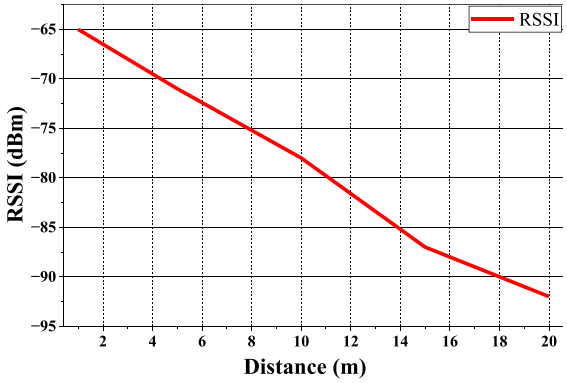

FIGURE 22. RSSI plot for range test of the ZigBee antenna.

real-world, over-the-air (OTA) performance of the proposed antenna in a realistic deployment scenario.

As depicted in Fig. 21, a range-test setup was established utilizing two XBee Configuration and Test Utility (XCTU)-configured ZigBee nodes. As summarized in Table 6 and plotted in Fig. 22, the measured RSSI predictably attenuated as the separation distance increased. Maintaining an average RSSI of approximately -69.4 dBm and a packet success rate of 84% under nominal interference conditions, the system demonstrated highly stable short-range communication.

Various antennas are compared and examined in Table 7 based on a number of factors, including substrate type, peak gain, impedance matching, and network validation, which will draw attention to the suggested antenna's features.

5. CONCLUSION

This paper offers the design and experimental validation of an ultra-thin, compact microstrip antenna resonating at 2.4 GHz for ZigBee-based IoT applications. Fabricated using an FR4 substrate with miniaturized dimensions of $20 \times 40 \times 0.8\,mm^3$, the antenna demonstrates excellent impedance matching. The simulated and measured results are very close, providing a measured return loss of -41 dB and bandwidth of 150 MHz, which incorporates the required ZigBee band. The designed antenna achieved a measured peak gain of 2.46 dBi and a radiation efficiency of 78%. Also, experimental integration with a ZigBee module validated strong short-range communication capabilities through RSSI calculation. Owing to its nominal structure, low physical profile, and economical fabrication, the suggested antenna is acceptable for IoT-enabled systems. However, the proposed design is limited to single-band operation, and future work will focus on dual-band functionality for short-range along with long-range communication by enabling simultaneous ZigBee and long-range (LoRa) communication. In addition, the inclusion of machine learning algorithms will facilitate deep data analysis and adaptive resource management along with these dynamic wireless networks.

REFERENCES

[1] Ndih, E. D. N. and S. Cherkaoui, "On enhancing technology coexistence in the IoT era: ZigBee and 802.11 case," *IEEE Access*, Vol. 4, 1835–1844, 2016.

[2] Mowla, M. N., N. Mowla, A. F. M. S. Shah, K. M. Rabie, and T. Shongwe, "Internet of Things and wireless sensor networks for smart agriculture applications: A survey," *IEEE Access*, Vol. 11, 145 813–145 852, 2023.

[3] Romputtal, A. and C. Phongcharoenpanich, "T-slot antennas-embedded ZigBee wireless sensor network system for IoT-enabled monitoring and control systems," *IEEE Internet of Things Journal*, Vol. 10, No. 23, 20 834–20 845, Dec. 2023.

[4] Yan, Y., A. Sharif, J. Ouyang, C. Zhang, and X. Ma, "UHF RFID handset antenna design with slant polarization for IoT and future 5G enabled smart cities applications using CM analysis," *IEEE*

Access, Vol. 8, 22 792–22 801, 2020.

[5] Arboleda, M. B., K. Klionovski, S. Zhen, and A. Shamim, "Orientation aware intelligent 3-D cubic antenna system with automated radiation pattern reconfigurability," *IEEE Open Journal of Antennas and Propagation*, Vol. 3, 812–823, 2022.

[6] Liao, C.-T., Z.-K. Yang, and H.-M. Chen, "Multiple integrated antennas for wearable fifth-generation communication and Internet of Things applications," *IEEE Access*, Vol. 9, 120 328–120 346, 2021.

[7] Islam, S., M. Zada, U. R. Iman, and H. Yoo, "Multibeam circular endfire array incorporating highly efficient nona-band rectifiers for IoT energy harvesting applications," *IEEE Internet of Things Journal*, Vol. 11, No. 12, 22 768–22 778, Jun. 2024.

[8] Musa, U., S. M. Shah, H. A. Majid, I. A. Mahadi, M. K. A. Rahim, M. S. Yahya, and Z. Z. Abidin, "Design and implementation of active antennas for IoT-based healthcare monitoring system," *IEEE Access*, Vol. 12, 48 453–48 471, 2024.

[9] Kiran, A. and G. K. Mishra, "Bluetooth, Wi-Fi, and Wi-Max supporting spectacles antenna for Internet of Things applications," *IEEE Internet of Things Journal*, Vol. 11, No. 21, 35 185–35 192, Nov. 2024.

[10] Rajavel, V. and D. Ghoshal, "A compact multiband frequency reconfigurable antenna integrated with sextuple band artificial magnetic conductor for heterogeneous wireless applications," *Frequenz*, Vol. 79, No. 3-4, 143–166, 2025.

[11] Hake, S., R. Jaiswal, S. Moon, P. Nikam, A. Bhosale, S. Mathad, and V. Yallapurmath, "Sub-ultra wideband ISM range patch antenna using foam substrate: A high-gain corner-cut design approach," *Russian Microelectronics*, Vol. 53, No. S1, S27–S35, 2024.

[12] Mahapatra, S. and M. N. Mohanty, "A review on state of art techniques of antennas for body area networks," *International Journal of Sensors Wireless Communications and Control*, Vol. 11, No. 6, 604–618, 2021.

[13] Abdulhussein, A. M., A. H. Khidhi, and A. A. Naser, "Omnidirectional microstrip patch antenna for 2.4 GHz wireless communications," in *Journal of Physics: Conference Series*, Vol. 2114, No. 1, 012051, Istanbul, Turkey, 2021.

[14] Almawgani, A. H. M., V. Sorathiya, and A. R. H. Alhawari, "Design of dipole array MIMO antenna for multiband and ultrawideband radiation applications in WiFi/Zigbee/WiMAX/satellite and mobile communications," *Applied Physics A*, Vol. 129, No. 6, 449, 2023.

[15] Mansour, M. M., M. Murakami, S. Torigoe, S. Yamamoto, and H. Kanaya, "Experimental demonstration of wireless energy harvesting for Zigbee wireless communication," in *2021 International Conference on Electronics Packaging (ICEP)*, 149–150, Tokyo, Japan, 2021.

[16] Bashir, U., K. R. Jha, G. Mishra, G. Singh, and S. K. Sharma, "Octahedron-shaped linearly polarized antenna for multistandard services including RFID and IoT," *IEEE Transactions on Antennas and Propagation*, Vol. 65, No. 7, 3364–3373, Jul. 2017.

[17] Hong, W., S. Lim, S. Ko, and Y. G. Kim, "Optically invisible antenna integrated within an OLED touch display panel for IoT applications," *IEEE Transactions on Antennas and Propagation*, Vol. 65, No. 7, 3750–3755, Jul. 2017.

[18] Li, G., Y. Huang, G. Gao, X. Wei, Z. Tian, and L.-A. Bian, "A handbag zipper antenna for the applications of body-centric wireless communications and Internet of Things," *IEEE Transactions on Antennas and Propagation*, Vol. 65, No. 10, 5137–5146, Oct. 2017.

[19] Islam, M. S., M. T. Islam, M. A. Ullah, G. K. Beng, N. Amin, and N. Misran, "A modified meander line microstrip patch antenna with enhanced bandwidth for 2.4 GHz ISM-band Internet of Things (IoT) applications," *IEEE Access*, Vol. 7, 127 850–127 861, 2019.

[20] De Cos Gómez, M. E., H. F. Alvarez, A. F. Berdasco, and F. L.-H. Andrés, "Paving the way to eco-friendly IoT antennas: Tencel-based ultra-thin compact monopole and its applications to ZigBee," *Sensors*, Vol. 20, No. 13, 3658, Jun. 2020.

[21] Dong, Y., J. Choi, and T. Itoh, "Folded strip/slot antenna with extended bandwidth for WLAN application," *IEEE Antennas and Wireless Propagation Letters*, Vol. 16, 673–676, 2017.